*Desalination and Water Treatment*
www.deswater.com

35 (2011) 14–32
November

1944-3994/1944-3986 
doi: 10/5004/dwt.2011.3126

# The scope to improve the efficiency of solar-powered reverse osmosis

T.Y. Qiu, P.A. Davies*

*Sustainable Environment Research Group, School of Engineering and Applied Science, Aston University, Birmingham B4 7ET, UK*
*Tel. +44 (0)121 204 3724; Fax: +44 (0)121 204 3683; email: p.a.davies@aston.ac.uk*

Received 1 November 2010; Accepted 6 May 2011

**ABSTRACT**

The aim of this paper is to identify and evaluate potential areas of technical improvement to solar-powered desalination systems that use reverse osmosis (RO). We compare ideal with real specific energy consumption (SEC) to pinpoint the causes of inefficiency. The ideal SEC is compared among different configurations including a batch system driven by a piston, and continuous systems with single or multiple stages with or without energy recovery in each case. For example, to desalinate 1 $m^3$ of freshwater from normal seawater (osmotic pressure 27 bar) will require at least 0.94 kWh of solar energy; thus in a sunny coastal location, up to 1850 $m^3$ of water per year per $m^2$ ($m^3/m^2$) of land covered by solar collectors could theoretically be desalinated. For brackish water (osmotic pressure 3 bar), 11570 $m^3/m^2$ of fresh water could theoretically be obtained under the same conditions. These ideal values are compared with practically achieved values reported in the literature. The practical energy consumption is found to be typically 40–200 times higher depending on feed water composition, system configuration and energy recovery. For state-of-the-art systems, energy losses at the various steps in the conversion process are quantified and presented with the help of Sankey diagrams. Improvements that could reduce the losses are discussed. Consequently, recommendations for areas of R&D are highlighted with particular reference to emerging technologies. It is concluded that there is considerable scope to improve the efficiency of solar-powered RO system.

*Keywords:* Solar power; Reverse osmosis; Photovoltaic; Rankine cycle; Specific energy consumption; Efficiency

## 1. Introduction

Water and energy are two essential elements to maintain life on the earth. Nowadays, nearly one fourth of mankind is suffering from fresh water shortage, and this situation will get worse as population increases [1]. The growing demand for fresh water, the environmental impacts of conventional desalination, and climate change are factors that call urgently for the desalination of seawater and brackish water using renewable energy sources (RESs). Nonetheless, although the coupling of RESs with desalination plants is promising and has been studied for years, plants using RESs remain mostly small in scale and represent only approximately 0.02% of the total world desalination capacity [2].

Desalination processes can be classified according to the type of energy source such as: (i) thermal energy, for example multi-effect desalination (MED) and multi-stage flash (MSF) technologies; (ii) electrical energy, for example electrodialysis (ED) technology and (iii) mechanical energy, for example reverse osmosis (RO) and vapour compression (VC) technologies. Among these desalination technologies, RO is a relatively new process, whose successful commercialization occurred

*Corresponding author.

in the early 1970s. Ever since, RO has been rapidly overtaking thermal desalination in terms of market share thanks to its relatively low initial investment, plant modularity, reduced environmental impact and short construction times [3]. More importantly, during RO desalination, there are no water phase changes and all energy is used to provide pressure to the saline feed, so the overall energy consumption of RO is much lower than that of MSF, MED and VC technologies [4].

There are three main RESs available and applicable to desalination: solar, wind and geothermal. For the purpose of desalination, geothermal energy is not as popular as the other two as it is available in few places, whereas wind and photovoltaic (PV) solar energies are more commonly coupled with RO desalination. Solar-driven RO desalination technology has been under development since the 1980s [5]. Most systems use either direct solar thermal energy to distil the water or PV conversion of sunlight to electricity followed by the use of the electricity in RO processes. Many experiments have been conducted on PV-RO desalination systems and practical implementations have been seen in many remote areas. Keeper et al. [6] reported one of the earliest PV-SWRO desalination systems with an energy recovery device (ERD) in 1985. The system achieved a specific electrical energy consumption below 4 kWh/m$^3$ of product water. In comparison, recent systems have achieved SECs of 2.32 kWh/m$^3$ [7].

To identify the performance of practical solar-powered RO desalination, this paper is going to review several noteworthy solar PV-RO and solar thermal-RO desalination systems. In particular it will compare their performances with the ideal cases and thus quantify the theoretical potential for improvement. Further, by evaluating the various energy losses occurring in the RO, PV and Rankine cycle subsystems, the paper will recommend about how to minimise these losses and thus ultimately increase the overall efficiency of future systems.

## 2. The reverse osmosis subsystem

### 2.1. Ideal vs. real energy usage of RO desalination

The ideal RO desalination process could be considered as a batch system as illustrated in Fig. 1, where the piston is the semi permeable membrane. As the piston is pushed towards the right side, only fresh water flows through the membrane, while salt is rejected. Assuming such an ideal batch RO system has 100% salt rejection and performs without any leakage, pressure or frictional losses, it will consume a theoretical minimum energy when it is utilized to desalinate a portion of salt solution. Ideally, this theoretical minimum work would only depend on the osmotic pressure $P_{osm}$ of the solution and the recovery ratio $r$, but needless to say, we cannot expect to achieve it in practice. Nevertheless, the theoretical minimum energy consumption provides a standard value against which to evaluate the performance of practical RO systems.

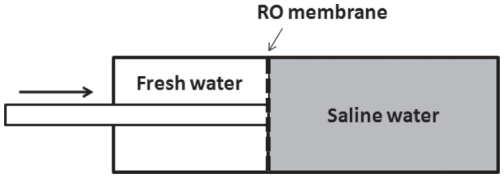


Fig. 1. An ideal RO batch desalination system.

For minimum energy consumption, the pressure applied to the solution should be just sufficient to overcome the osmotic pressure. Since the bulk concentration increases as freshwater is extracted through the RO membrane, the osmotic pressure $P_{osm}$ of the solution increases correspondingly; thus, the theoretical energy of desalination depends not only on the osmotic pressure but also on the fraction recovery $r$ of pure water removed from the solution. If the water permeating the membrane is completely free of salt, the theoretical minimum work $W$ to desalinate a volume $V$ of feed solution is given:

$$W = P_{osm} V \ln\left(\frac{1}{1-r}\right) \tag{1}$$

So, the ideal $SEC$ corresponding to mechanical work (or electricity) per unit volume of recovered solution is:

$$SEC_{ideal} = P_{osm} \frac{1}{r} \ln \frac{1}{(1-r)} \tag{2}$$

Thus, for a desalination process driven by solar energy, the ideal solar energy usage is:

$$SEC_{ideal} = P_{osm} \frac{1}{r}\left[\ln \frac{1}{(1-r)}\right] \frac{1}{\eta_{solar}} \tag{3}$$

where $\eta_{solar}$ is the ideal efficiency of solar energy conversion to mechanical work, which is equal to 86.8%, as will be explained in Section 3 [8].

For instance, to desalinate 1 m$^3$ of freshwater from normal seawater, with osmotic pressure 27 bar, at recovery ratio of 25% will ideally require just 0.94 kWh of solar energy, which indicates that in a sunny coastal location receiving 7200 MJ/m$^2$/y, up to 1850 m$^3$ of water per year per m$^2$ of land covered by solar collectors could theoretically be desalinated. To desalinate brackish water, with osmotic pressure 3 bar and 50% recovery ratio, 11570 m$^3$ of fresh water could theoretically be obtained under the

same conditions. Now according to the US reference daily intake, drinking water per person per day must be at least 2.7 l [9]. If the ideal solar-RO system were realized, 1 $m^2$ of solar collector could therefore desalinate enough seawater to provide drinking water for 1850 people. This emphasises the potential of solar-powered desalination to provide abundant clean water in arid coastal areas.

In practice, the electrical energy requirement for SWRO desalination systems coupled with renewable energy is usually in the range 7–15 kWh/$m^3$. With ERDs, this value can be reduced to below 5 kWh/$m^3$. For brackish water, the minimum SEC (for feed water of osmotic pressure 2.7 bar) with 70% recovery ratio is 0.15 kWh/$m^3$. Nevertheless, the practical SEC of brackish water systems is 1–3 kWh/$m^3$ [10,11].

Table 1 reviews PV-RO systems for seawater and brackish water desalination which were built in the last 10 y and exhibited good performance. Based on the assumptions mentioned before, the theoretical minimum SEC for each system in Table 1 can be obtained from Eq. (3). The solar energy available for desalination = solar irradiance × PV panel area; thus, the actual solar energy usage equals the total input solar energy divided by the fresh water production. We define the efficiency ratio $r_\eta$ as the ideal energy usage divided by the actual solar energy usage.

There are several reasons why the energy needed is in practice significantly greater than the theoretical minimum. Many losses occur through the desalination process, whereby the supplied energy – instead of being converted into the free energy of the separated components of the salt solution – is lost to the surroundings in some non-useful form such as heat. Due to these losses in the RO system and, moreover, other losses in the PV system, the efficiency of PV-RO desalination system are quiet low compared to the ideal cases. Table 1 shows that even the best existing systems may theoretically be improved some 40 times for seawater and 200 times for brackish water. The main losses in an RO system are discussed in the next sections.

### 2.2. Energy losses

RO is a filtration method that uses a semi-permeable membrane to remove salt from feed water. A typical PV-RO system operates using a high pressure pump which is powered by electricity from PV panels, and imparts high pressure to the feed water, thus forcing feed water to overcome the osmosis pressure and flow through the membrane surface. The Sankey diagram of Fig. 2 shows the different types of energy losses during this operation. Note that this diagram represents the situation without any ERD. The amount of crossflow losses are determined by membrane properties, concentration polarization (CP) and longitudinal concentration increase phenomena. On the left side, the total input electrical energy is denoted as 100%; but after successive losses, the essential energy of desalination is just 2.5%. Firstly, we will discuss the inverter and pump losses and then the losses in RO system.

Table 1
Overview some of the outstanding PV-RO systems

| Author, year and source | Feed water (ppm) | Recovery ratio | Ideal solar energy usage (kWh/$m^3$) | PV material | PV capacity ($kW_p$) | Energy recovery device | Actual solar energy usage (kWh/$m^3$) | Efficiency ratio ($r_\eta$) |
|---|---|---|---|---|---|---|---|---|
| Mohammed et al., 2006 [12,13] | 30425 | 0.1 | 0.82 | Mono Si | 0.85 | Clark pump | 54.7 | 0.015 |
| Herold et al., 2006 [14,15] | 35500 | 0.15 | 0.98 | Mono Si | 4.8 | No | 75.4 | 0.013 |
| Mohamed et al., 2003 [16] | 40000 | 0.23 | 1.16 | Mono Si | 31.2 | Brine hydraulic | 114.2 | 0.01 |
| Thomson et al., 2003 [17] | 29000 | 0.1 | 0.78 | Mono Si | 1.53 | Clark pump | 34.7 | 0.023 |
| Tzen et al., [18] | 40000 | 0.23 | 1.16 | Multi Si | 26.3 | Yes | 34.2 | 0.034 |
| Joyce et al., 2000 [19] | 2549 | 0.02 | 0.07 | – | 0.15 | No | 343.7 | 0.0002 |
| Qiblawey et al., 2007 | 720 | 0.37 | 0.02 | Mono Si | 0.11 | No | 110.5 | 0.0002 |
| Ahmad et al., 2000 [20] | 2000 | 0.5 | 0.07 | Mono Si | 1.1 | No | 55 | 0.0013 |
| Carvalho, 2000 [21] | 1200 | 0.27 | 0.04 | – | 1.1 | No | 8.9 | 0.004 |
| Munari et al., 2005 [22] | 3982 | 0.18 | 0.11 | Multi Si | 0.6 | No | 90.2 | 0.0012 |
| Richards et al., 2003 [23] | 3500 | 0.55 | 0.13 | Mono Si | 0.26 | No | 25.4 | 0.005 |
| Riffel et al., 2006 [24] | 800 | 0.13 | 0.02 | – | 0.17 | No | 30.9 | 0.0007 |

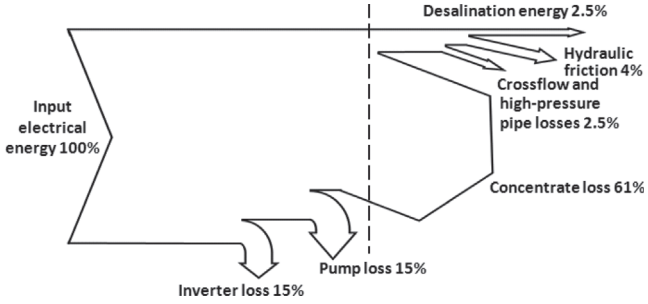


Fig. 2. Sankey diagram showing various energy losses in a typical seawater RO system.

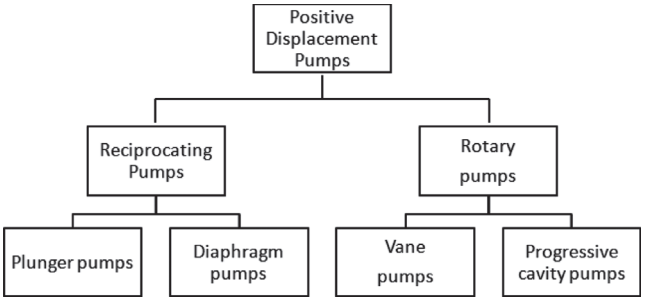


Fig. 3. Types of positive displacement pumps.

*2.2.1. Motor and pump losses*

The first set of losses is associated with the conversion of the supplied energy, typically in the form of electricity or shaft work, into mechanical work acting on the solution. The latter can be referred to as hydraulic work and is equivalent to the pressure of the solution multiplied by the volumetric flow at which it is supplied to the RO membranes. Though electrical energy or shaft work can in theory be converted to hydraulic work with 100% efficiency by means of a motor and pump, in practice several losses occur. In a PV-RO system, since all of the electrical energy is consumed by the high pressure pump, pump selection becomes a crucial issue. The high-pressure pump should provide just enough power to get a continuous, defined ideal flow rate of permeate flow without extra energy wastage.

The losses in the pump will depend on the type of pump used. In a centrifugal pump, for example, clearances around the pump rotor allow some of the fluid to flow in the reverse direction. Shearing of the fluid between the rotor and casing is another source of loss. Franca et al. also pointed out that high pressure centrifugal pumps easily tended to corrode in the salty solution without proper design, resulting in a gradual deterioration of efficiency to values as low as 40% [25].

In general, positive displacement pumps and centrifugal pumps are used in RO systems. These two types of pumps behave very differently regarding pressure head and flow rate. The positive displacement pumps, unlike the centrifugal pumps, produce constant flow at a given speed regardless of the system pressure, and have higher hydraulic efficiency than centrifugal pumps. However, their output capacities are limited and they require more frequent maintenance than centrifugal pumps [26]. Positive displacement pumps are always used in small capacity systems and their efficiency can achieve 90%, which is a distinct advantage compared to 65–75% efficiency of centrifugal pumps. Fig. 3 shows the categories of positive displacement pumps. In batteryless PV-RO desalination systems, the available power varies with solar irradiance, so positive displacement pumps are better suited. Nevertheless, in large capacity RO systems, centrifugal pumps are exclusively used, due to their almost unlimited capacity; moreover, at higher RO feed flows, the efficiency of such pumps can reach 84–88% [27].

As regards electric motors, these are subject to losses due to electrical resistance in the windings, friction caused by air interacting with the rotor and electromagnetic losses to the surroundings. The shaft connecting the motor to the pump will be subject to friction from the bearing supporting it. Operation conditions also affect their performance, which can be improved by setting optimum operation parameters. The high pressure pump preferably should be operated with a DC motor, directly connected to the solar-PV panel via a buffering battery, whereas AC operation would add a further loss through the need for a DC/AC converter.

*2.2.2. Energy loss in concentrate*

The second type of loss associated with the RO system has to do with energy recovery from the concentrated solution that leaves the RO module. Since the brine pressure is only slightly lower than the operating pressure, the energy loss in the rejected brine can be a major part of the overall losses. To recover the large amount of energy in the brine is an efficient way to minimize energy consumption and eventually to improve the efficiency of RO desalination systems. Thus, it is desirable to reuse the energy contained in the brine by means of an ERD. The specific electrical energy consumption of RO desalination has been decreased significantly over the past decades with the help of improved ERDs.

Over the years, varieties of ERDs have been developed and implemented for RO systems [13,28–34]. In 1980, the first large municipal SWRO desalination plant began operating in Jeddah, Saudi Arabia. Without ERD, it consumed about 8 kWh/m$^3$ [35]. Then Francis turbines were introduced for energy recovery. Taking as an example the desalination plant at Las Palmas, in the Canary Islands, the implementation of the Francis turbine enabled the energy consumption of the plant to

be lowered to 5 kWh/m$^3$. In the later 1980s, Francis turbines were replaced by Pelton turbines due to the higher efficiency of the latter. Since the 1990s, another type of ERD, the hydraulic turbocharger, has become popular. They are similar in concept to the Pelton turbine, but the difference is they are not directly connected to the high-pressure pump, resulting in flexibility of operation and a slightly higher efficiency of 80%. Pressure exchanger ERDs have been developed in the last 15 y. The piston type pressure exchanger has high efficiency of 95%, which enables it to lower the SEC of a desalination system to 3 kWh/m$^3$ [36]. Moreover their efficiency is relatively constant despite flow and pressure variations and is independent of device capacity. The rotary type pressure exchanger ERD, which has a higher efficiency up to 98%, may lower energy consumption even further [37]. Energy Recovery Inc. claims that their ERI PX Pressure Exchanger can reduce the amount of energy required in seawater desalination by up to 60%, to as low as around 1.7 kWh/m$^3$ [38]. Fig. 4 represents the energy consumption of some desalination systems which adopted different ERDs together with the efficiency of these ERDs.

However, previous work showed that ERDs are more suited to seawater systems than to the brackish water systems due to the much lower operation pressure of the latter [35,37,39]. Moreover, unless 100% of this energy is recovered and used to assist the feed pump, the ideal minimum of Eq. (2) cannot be achieved. Depending on the type of ERD used, the actual energy recovered may be somewhat less than the ideal amount. In smaller systems energy recovery may be absent altogether. There is a great opportunity to improve the efficiency of brackish water desalination systems, especially smaller systems, through the implementation of ERDs.

A further set of losses is associated with the fact that the pressure needed in the RO system is, in practice, significantly greater than the ideal minimum. There are three main causes of this as explained in the following sections.

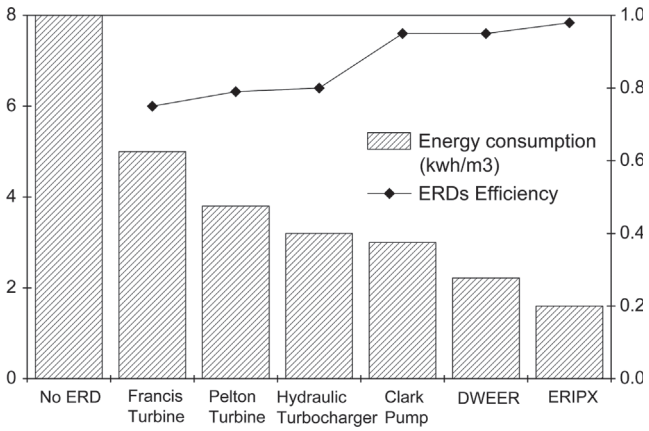


Fig. 4. Energy consumptions of systems adopting different ERDs and efficiencies of ERDs.

### 2.2.3. Concentration polarization

In the RO process, the flux of water through the membrane results in a build up of salts near the membrane surface. Thus, the salt concentration near the surface of the membrane exceeds that in the bulk of the solution by a factor $C_p$. This transverse gradient of concentration across the channel enclosed by the membranes is referred to as concentration polarisation and is illustrated in Fig. 5. Since the osmotic pressure is, to a good approximation, proportional to the concentration it can be expected that the required operation pressure will be increased by the factor $C_p$, and the operation pressure and pumping power requirements will be increased correspondingly. Moreover CP can cause many other negative effects on the RO process, such as decreasing permeate flux and increasing salinity of the product water [40,41].

In order to understand the CP phenomenon and minimize its negative influence on energy efficiency, some models have been established to explain the solute transport mechanisms. In 1970, Michaels and co-workers provided the first comprehensive analysis of CP in ultrafiltration, and Porter proposed the *gel-polarization model* to explain the effects of CP [42,43]. Many other researchers have studied this phenomenon and pointed out several fundamental models applicable to ultrafiltration and RO [44–46]. Among these models, the film theory is the most classic one, since it provides a simple analytical approach that works well for most RO separations. Therefore, film theory has been applied as the design basis for most modern RO processes.

The film model proposed by Sourirajan is:

$$J = k \ln\left(\frac{c_m - c_p}{c_b - c_p}\right) \tag{4}$$

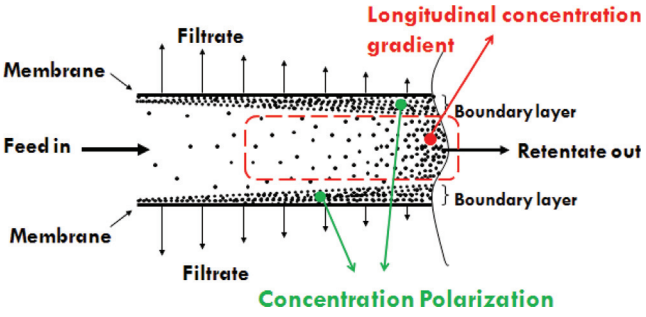


Fig. 5. The phenomenon of concentration polarization and longitudinal concentration gradient in membrane filtration.

where $J$ is the water flux (cm/s), $k$ is the mass transfer coefficient, $C_m$ is the membrane surface salt concentration and $C_b$ is the bulk salt concentration [47]. This expression can be rearranged to provide a direct estimation of the concentration polarisation modulus ($C_m/C_b$) from:

$$\frac{c_m}{c_b} = (1 - R_0) + R_0 \exp\left(\frac{1}{k}\right) \quad (5)$$

where $R_0$ is the salt rejection.

Since the 1970s, many researchers have simulated CP in RO channels based on film theory models and solution diffusion models [8,48,49]. But the majority of these models are based on filtration in flat channels; therefore they are simplified cases compared to practical RO spiral wound modules which are the most popular modules used in desalination today. The mathematical analysis of spiral wound modules needs to take into account the three-dimensional geometry of the feed and permeate channels and their spacers. Thus, the mass transfer coefficient $k$ is a function of the physical properties of the geometry and the fluid flow. Chiolle proposed an equation to calculate the mass transfer coefficient $k$ in a RO channel equipped with a spacer, which was proved by experiments [50,51]:

$$k = 0.753\left(\frac{K}{2-K}\right)^{1/2}\frac{D}{h}Sc^{-1/6}\left(\frac{Peh}{M}\right)^{1/2} \quad (6)$$

where $K$ is the mixing efficiency of the net, $M$ is the characteristic length of net, $Sc$ is the Schmidt number ($v/D$) (ν is velocity), $Pe$ is the Peclet number ($\mu h/D$) (μ is viscosity, $h$ is height of the channel), and $D$ is the diffusion coefficient of the solute ($m^2/s$).

From Eqs. (5) and (6), it is obvious that the concentration at the membrane surface depends upon the flux through the membrane, the retention of the membrane, the diffusion coefficient of the solute $D$ and the thickness of the concentration boundary layer. Intrinsically, CP is highly related to the feed velocity, feed concentration, applied pressure and operating temperature [52].

Based on the mechanism of CP, there are two types of method that could be adopted to reduce it: (i) increase of membrane cross flow velocity, but this requires more energy and may be limited due to the pressure drop along the channel; (ii) increase of mass transport, which can be done by new design concept of RO modules, such as adding turbulence promoters, rotating and vibrating membranes.

### 2.2.4. Longitudinal concentration increase

Aside from the transverse gradient of salt concentration mentioned in the last section, there also occurs a longitudinal gradient of concentration as the water is progressively removed from the solution while it moves along the membrane channel. For the case of seawater desalination with an inlet flow velocity of 0.08 m/s, Fig. 6 (based on reference [50]) shows the longitudinal concentration and the pressure changes along the channel. Similar to the CP phenomenon, the osmotic pressure increases with the increasing longitudinal concentration along the channel. Therefore, in order to maintain a flux of water over the entire membrane surface, the solution must be pressurised according to the concentration at the outlet, even though this exceeds the pressure required at the inlet where the concentration is the least.

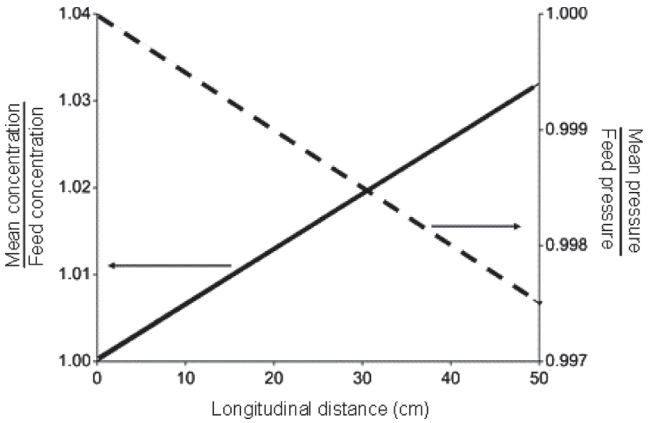


Fig. 6. Feed water mean concentration and pressure changes along channel longitudinal distance.

One possible approach to minimize the effect of longitudinal concentration gradient is to divide one whole channel into several stages in series, with intermediate pumps to apply the appropriate pressure to each one. Table 2 lists the expressions for SEC and efficiency ratio for RO systems with different numbers of stages. Based on these formulae, Fig. 7 plots the theoretical efficiency ratios vs. the recovery ratios. It is seen that the multi-stage RO system achieves higher efficiency than its counterparts with fewer stages. To achieve the ideal minimum energy usage, the number of serial stages should theoretically be infinite, which is infeasible in practice, thus there will remain in practice some loses associated with the longitudinal concentration gradient. However, for a recovery of 50%, the 3-stages system will increase the efficiency ratio by 12.4%, which is a significant improvement.

### 2.2.5. Excess pressure to overcome hydraulic friction

Even if transverse CP could be eliminated, and the effects of longitudinal concentration gradient minimised, a third reason why the pressure across the membrane needs to be greater than the local osmotic pressure is to overcome the hydraulic friction of the membrane.

Table 2
Specific energy consumptions and efficiency ratios for different RO system configurations operating at recovery rate $r$ (single stage) or overall recovery rate $R$ for more than one stage

| RO system configuration | Without energy recovery | | With energy recovery | |
|---|---|---|---|---|
| | Specific energy consumption | Efficiency ratio ($r_\eta$) | Specific energy consumption | Efficiency ratio ($r_\eta$) |
| Single stage | $P_{osm}\frac{1}{r(1-r)}$ | $(1-r)\ln\frac{1}{(1-r)}$ | $P_{osm}\frac{1}{(1-r)}$ | $\frac{(1-r)}{r}\ln\frac{1}{(1-r)}$ |
| Two stages | $\frac{P_{osm}}{R}\left(\frac{2}{\sqrt[2]{1-R}}-1\right)$ | $\frac{\ln[1/(1-R)]}{\left(\frac{2}{\sqrt[2]{1-R}}-1\right)}$ | $P_{osm}\left(\frac{2}{\sqrt[2]{1-R}}-2\right)$ | $\frac{\ln[1/(1-R)]}{2\left(\frac{1}{\sqrt[2]{1-R}}-1\right)}$ |
| $n$ stages | $P_{osm}\left[\frac{n}{\sqrt[n]{1-R}}-(n-1)\right]$ | $\frac{\ln[1/(1-R)]}{\left[\frac{n}{\sqrt[n]{1-R}}-(n-1)\right]}$ | $P_{osm}\left(\frac{n}{\sqrt[n]{1-R}}-n\right)$ | $\frac{\ln[1/(1-R)]}{n\left(\frac{1}{\sqrt[n]{1-R}}-1\right)}$ |

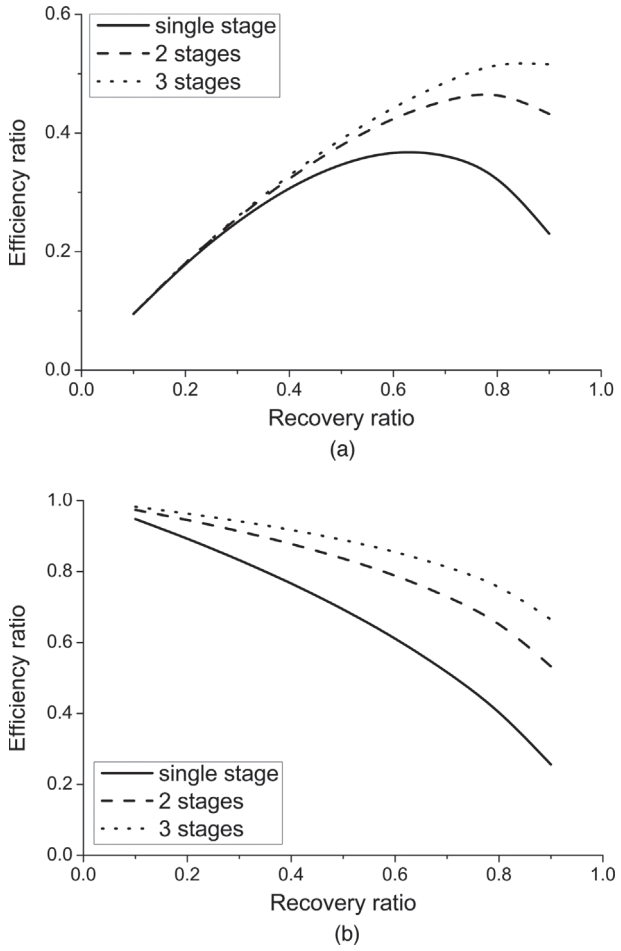


Fig. 7. Efficiency ratio of different RO system configurations: (a) system without ERD (b) system with ERD.

The membrane is not infinitely permeable to pure water; instead some differential pressure is needed to drive a finite flux. This can only be eliminated by making the area of membrane very large which, aside from being costly, would result in a significant passage of salt through the membrane such that the permeate would become less pure. Thus in practice there is always some energy loss associated with the hydraulic friction of the membrane. Nevertheless, choosing the most suitable membrane could reduce the energy loss related to membrane resistance.

The required energy and pressure are dependent on the feed water concentration and the permeate flow rate which are determined by the permeation characteristics of the membrane material and its molecular structure. For the same recovery ratio, membranes having a high permeability with similar salt rejection capabilities enable a reduction in hydraulic friction of membrane and lead to energy consumption reduction. Fig. 8 illustrates the required energy to desalinate a 3000 ppm NaCl solution for different types of membranes (simplified from [11] Fig. 4). These membranes have similar salt rejection rate; however the energy consumptions vary widely from 0.48 kWh/m$^3$ for the ESNA type membrane to 3 kWh/m$^3$ for the CAB type membrane.

A further hydraulic loss may be associated with the friction of the fluid flowing along the channel. The pressure at the inlet to the RO module is in practice slightly greater than that at the outlet whereas ideally these two pressures should be equal. However, this loss is in practice likely to be small compared to the other three pressure-related losses mentioned above.

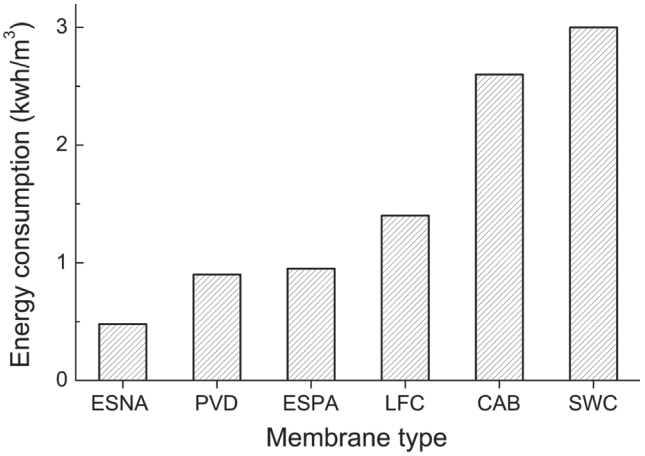


Fig. 8. Energy consumption VS different membrane type, ESNA: softening membranes, PVD: polyvinyl alcohol derivative membrane, ESPA: low-pressure membranes, LFC: low-fouling membranes, CAB: blend cellulose acetate membrane, SWC: seawater membrane.

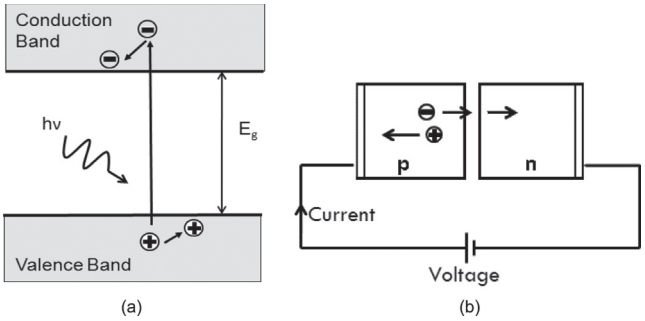


Fig. 9. For a typical conventional crystalline silicon solar cell (a) the electron-hole pair generation, (b) electrons collection.

## 3. The photovoltaic subsystem

In a PV-RO desalination system, aside from the various losses happening in the RO system, the inefficiency of the PV system also lowers the system performance. The next sections give an overview of PV solar cells, the losses occurring in them, and potential methods to reduce these losses.

### *3.1. The physical basis of PV solar cell operation*

In PV-RO applications, PV modules and panels are formed by connecting and encapsulating numerous solar cell units. Solar cells are made from solar PV materials which are semiconductors. Generally, PV energy conversion consists of two essential steps as shown in Fig. 9: (i) electron-hole pair generation: because the semiconductor materials have weakly bonded electrons occupying valence band, once photons are absorbed by these electrons, they can jump over the energy gap, and move to conduction band; (ii) electron collection: the generated electrons and holes are separated and collected by the structure of solar cell and electricity is thus conducted through the solar cell.

Most commercial solar cells are made of mono- or multi-crystalline silicon; these accounted for 90% of the world market in 2000 [53]. Other materials employed include amorphous silicon, cadmium telluride and even polymers. Solar cell developments have already been through three generations. The first generation was based on silicon wafers, which still dominate the solar cell market thanks to their high efficiency. In early 1980s, thin-film solar cells started to show promise and these became known as the second generation. Thin-film solar cells are super light and flexible, although they do not have advantages regarding efficiency compared to silicon solar cells, they do save a lot of materials, therefore cutting costs. And now researchers are trying to invent and develop novel designed solar cells of the so-called 'third generation' that have both higher efficiency and lower cost [54]. This generation represents the cutting edge of solar technology and with operating principles quite different from the traditional semiconductor p-n junction. The third generation includes emerging solar cells such as polymer solar cells, dye-sensitized solar cells, etc, and the research on them is still at a very early stage.

### *3.2. The efficiency of solar cells*

The Carnot limit applied to solar energy conversion suggests an efficiency of $1 - (T_1/T_2)$ (where $T_1$ is the temperature of the ambient conditions, which is assumed 300 K, $T_2$ is the temperature of the sun which is about 6000 K) implying that 95% may be possible. In fact, the conversion from sunlight to electricity necessarily has efficiency lower than this value, because solar energy capture is necessarily an irreversible process.

In 1950s, two sets of pioneers Trivich and Flinn and Shockley and Queisser calculated the 30% fundamental upper limit for single junction solar cells [55,56]. After that, more complete analyses of the theoretical limits of solar cells were given by Mathers and Ruppel [57,58]. In addition, several authors studied the efficiency limit of tandem solar cell structure since 1970s; and finally the maximum efficiency limit of 86.8% was concluded for infinite number of stacked solar cells in concentrated sunlight as shown in Table 3 [8,59–62].

As regards the efficiencies of real solar cells, Charles Fritts created the first prototype in 1883 with an efficiency of just 1% [63]. It was made of selenium and coated with a thin layer of gold. With the contribution of many scientists and researchers, solar cells efficiencies

Table 3
The maximum efficiencies of tandem cells as a function of the number of stacked cells, from [8]

| Unconcentrated sunlight | | Concentrated sunlight (ratio 45900: 1) | |
|---|---|---|---|
| Number of stacked cells | Maximum efficiency (%) | Number of stacked cells | Maximum efficiency (%) |
| 1 | 30 | 1 | 40 |
| 2 | 42 | 2 | 55 |
| 3 | 49 | 3 | 63 |
| … | … | … | … |
| ∞ | 68.2 | ∞ | 86.8 |

have improved gradually ever since. Take the mono-crystalline silicon solar cell as an example: its efficiency was only about 5% at the beginning of 1950s, increased to 14% in 1960, reached 16% in 1968, and finally 24.4% was achieved in silicon in 1998, which is still the best silicon solar cell efficiency measured under laboratory conditions [64–66].

Generally, commercial solar cells perform with lower efficiencies than the laboratory test values due to mass production and undesirable operation conditions. For instance, most of the mono-crystalline silicon PV panels employed by practical PV-RO desalination systems have an average efficient around 13%, in contrast to the best silicon solar cells which possess over 20% efficiency. Fig. 10 collates the best solar cells efficiencies achieved in recent decades for all the major PV technologies.

A multi-junction solar cell is made of more than one high purity crystalline material and can therefore capture a wide range of the solar spectrum (see Section 3.3.1below). Consequently, these cells perform with higher efficiency than the other kinds of cells, albeit at higher cost.

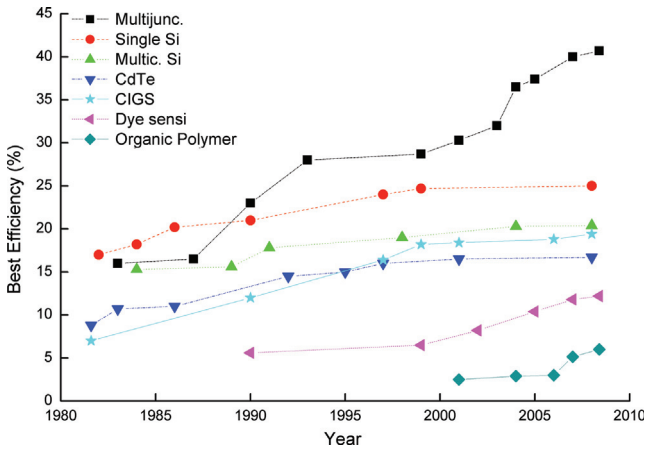


Fig. 10. The trends in best efficiency achieved over the past decades.

Regarding the minority materials used in PV technology, thin-film solar cells are becoming promising. They include Cu(InGa)Se(CIGS), CdTe and so on. Though their efficiencies are slightly worse than for silicon, nevertheless they have advantages with respect to cost due to their configuration. The third generation solar cells such as organic polymer and dye sensitized solar cells are less than 10% efficient.

### 3.3. Losses in solar cells

From the large difference between real solar cell efficiencies (Fig. 10) and the theoretical limit of 86.8%, it is evident that various losses happen during the conversion process of sunlight to electricity. There exist huge possibilities to improve the performance of solar cells. Fig. 11 presents a Sankey diagram showing the typical losses occurring in a high-performance silicon solar cell. The total input solar energy is denoted as 100%; but after successive losses, the actual energy output is only 23%.

In order to identify ways to minimise these losses to increase solar cell efficiency, and therefore ultimately improving PV-RO desalination system performance, in the following sections possible losses are pointed out together with recommendations. The discussions are based on silicon solar cells as this is the type used in almost all PV-RO systems today.

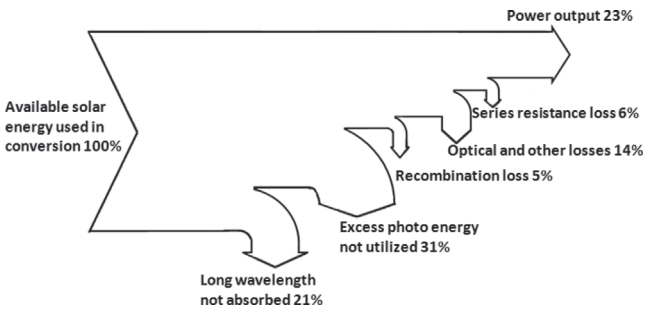


Fig. 11. Various energy losses in a silicon solar cell.

*3.3.1. Utilization of only part of solar energy*

Sunlight is a spectrum of photons of energies distributed over a wide range. For a semiconductor which has a single energy band gap, only the photons whose wavelengths are the same as the band gap can create an electron-hole pair without further loss of energy. In fact, a large number of the photons that will be absorbed will have more energy than is needed to create an electron-hole pair. Any energy that a photon has in excess of the energy gap of the material will not be utilized in the conversion process; instead, it contributes to the lattice vibrations of the material and will eventually be dissipated as heat. The other photons whose energy are less than the energy gap of the semiconductor do not contribute at all to electron-hole pair generations because they will go straight through the semiconductor; thus their energy is lost. The magnitudes of these two losses depend on the band gap of the semiconductor, which therefore has a big influence on solar cell efficiency. It is found that the most suitable band gap for absorbing sunlight is in the range 1.0–1.6 eV [67]. Therefore, for a silicon solar cell whose band gap is 1.1 eV, two large losses occur because of its poor utilization of solar energy: 21% of the available solar energy is wasted due to the photon energy being too low and 31% of the incident energy is dissipated as heat inside the silicon because the photon energy is too high. These are basic physical losses and governed by the semiconductor material.

To match more closely the energy spectrum of the sun, i.e., absorb as much solar energy as possible, semiconductor materials of different band gaps can be stacked together to form a much more efficient solar cell structure, i.e., multi-junction solar cell as shown in Fig. 12. Higher band gap semiconductors at the top of the stack absorb higher energy photons, allowing photons of energy less than their band gap to pass through; then, semiconductors beneath of lower band gaps absorb these photons. Thus, this approach could minimise the magnitude of the losses mentioned above, increase the overall conversion efficiency of solar cells. For example, single band gap GaAs solar cells have efficiency up to 26.2%, whereas the efficiency can be increased to 30% with double band gap GaInP/GaAs cells [68,69].

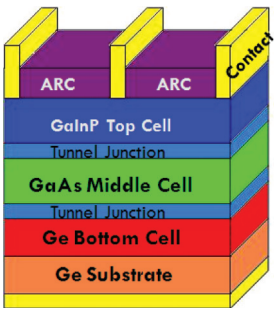


Fig. 12. A multi-junction solar cell.

*3.3.2. Recombination losses*

When a semiconductor is illuminated by a photon and electron-hole pairs are generated, not all the electron-hole pairs are created within the charged region of the p-n junction. Only those pairs created within a diffusion length of the junction can be collected and separated. Instead of being collected, the electrons and holes tend to relax back toward their equilibrium state through recombination process. Thus, recombination is the opposite process to carrier generation. It affects both the output current and the voltage of a solar cell, reducing its efficiency.

There are three types of recombination mechanisms as shown in Fig. 13.

a) Radiative recombination

Radiative recombination is simply the inverse of the generation process of electron-hole pairs. It happens in the body of the cell, when an electron falls from the conduction band down to the valence band, giving the

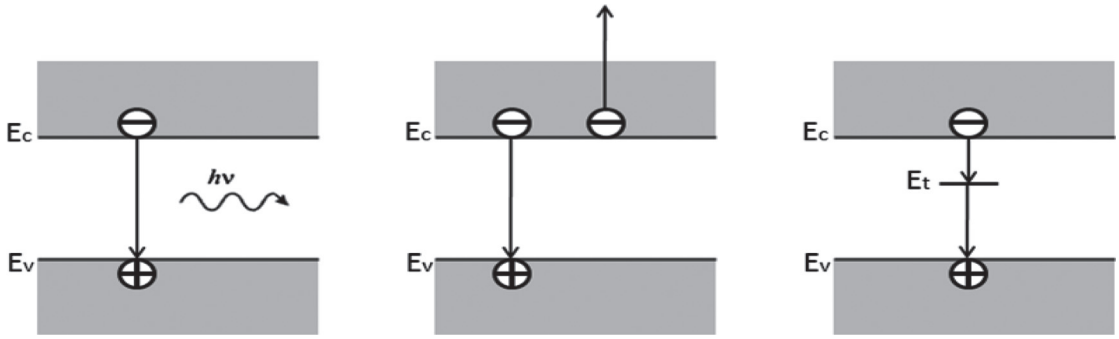


Fig. 13. Three types of recombination losses: (a) radiative recombination; (b) Auger recombination; (c) defect mediated recombination.

energy to an emitted photon, which is called spontaneous emission (this is how semiconductor lasers and light emitting diodes operate).

Radiative recombination is more prominent in direct band gap materials like gallium arsenide (GaAs) than indirect band gap materials like silicon due to the direct transitions from conduction band to valence band [70]. For instance, the coefficient of the radiative recombination rate of silicon material is $1.8\times10^{-21}$ $m^3/s$, which is much smaller than GaAs's coefficient of $7.2\times10^{-16}$ $m^3/s$.

b) Auger recombination

Auger recombination is similar to radiative recombination except that instead of emitting the energy away, the energy is given to another carrier, in either the conduction band or the valence band. Thus, the electron, or the hole release its excess energy and back down to the conduction or valence band edge.

From the mechanism of Auger recombination, it is clear that the intrinsic carrier concentration affects Auger recombination. In silicon, whose intrinsic carrier concentration is $1\times10^4$ $m^{-3}$, Auger recombination is much faster than in GaAs whose intrinsic carrier concentration is only 2 $m^{-3}$. Green demonstrated that Auger recombination, rather than radiative recombination, can pose the most severe intrinsic limitation on output current [71].

c) Defect mediated recombination

This type of recombination is also called Shockley-Read-Hall (SHR) recombination. It happens commonly at impurities or defects in cell body, or at the surface of the semiconductor where energy levels may be introduced inside the energy gap. These levels act as obstacles for the electrons to fall back into the valence band and recombine with holes. The interface recombination leads to lowering of both output current and voltage, as well as fill factor [72].

Surface recombination can be reduced by adapting and refining the PV device structure. For instance, Kosyachenko and Grushko proposed that the interface recombination and the recombination in the deletion layer could be eliminated with an appropriate barrier structure and material parameters: the carrier lifetime and the concentration of uncompensated impurities were in excess of and $10^{-8}$ s and $10^{22}$ $m^{-3}$ respectively, after investigating and analyzing these two types of recombination in thin-film CdS/CdTe PV devices [73].

Although recombination accounts for a small fraction of all losses, it reduces both the voltage and current output of the solar cell [74]. Over the decades, much research work has been done to reduce recombination losses. Researchers have proved that surface passivation of unmetallized regions on solar cells is a good way to reduce surface recombination [75,76]. It is also possible to reduce recombination at the external surfaces by chemical treatment with a thin layer of passivation oxide. For silicon solar cells, by designing low metal contact areas through heavily doping the surface of the silicon beneath the metal contact, the rear surface can be passivated to reduce recombination.

*3.3.3. Optical losses*

Semiconductor materials such as silicon are naturally shiny, causing reflection losses at the solar cell surface. In addition, light can be blocked and reflected by the contacts. Optical losses reduce the incident sunlight directly, thus lowering the production of electron-hole pairs.

Optical losses can be minimised by technical improvements. Shadowing can be reduced by minimising the total contact area but small contact area means large electrical resistance. The main challenge is to achieve a trade-off between them by new design technology. For instance, by using laser-formed grooves to define the metallisation pattern of the contact, one can make the contact narrower and deeper just below the cell's surface [67]. As regards reflection losses, these can be reduced by the addition to the top surface of a transparent anti-reflection coating (ARC) with appropriate thickness. Cid et al. reported a single layer anti-reflection coating which made the top surface reflection of the cell less than 10%. They also demonstrated that further reduction were achieved by the application of two or more ARC layers [77].

Surface texturing is another technique for reducing reflection losses. Basically, any roughness of the top surface would help reduce this kind of reflection loss. Zhao et al. obtained an increase in the efficiency of a multi-crystalline silicon solar cell from 18.6% to 19.8% by enshrouding cell surfaces in thermally grown oxide and from isotropic etching to form an hexagonally symmetric 'honeycomb' surface texture [78]. Additionally, 'raised pyramids' or 'inverted pyramids' surface pattern also can be utilized to give reflected light more chances to be absorbed by solar cell, thus reducing reflection losses as well as substantially increasing the cell's effective optical thickness by trapping light within the cell body [79,80]. Yoshikawa and Kasai reported that, by using optimized double anti-reflection coating layers, they reduced the reflection loss of a GaAlAs-GaAs solar cell to as low as 1.09% [81]. With pyramids, when combined with a single-layer ARC, the reflectivity of the top surface can be brought down to 1%.

*3.3.4. Series resistance losses*

The final efficiency loss shown in Fig. 11 is due to electrical resistance. The series resistance occurs in the fingers and bus bar, contacts, emitter and bulk resistance.

It has been found that in actual converters the series resistance of the cell can cause deviation from the ideal voltage-current characteristics. This deviation causes the characteristic curve to flatten resulting in a reduction in the net power output. Thus the effect of series resistance is manifested as a reduction in fill factor and output power.

Series resistance losses can be minimized by appropriate design of the solar cell structure. For instance, metal contact resistance is decided by fingers thickness, therefore by adding more and thinner fingers instead of less and thicker fingers, one will reduce resistance and increase current output.

The techniques for reducing the efficiency losses covered above have been conceived and enhanced over many years in R&D laboratories around the world, leading to continuous improvements in solar cell and PV module efficiencies. After further refinements, these losses may be reduced by a further 10% or so, which will enable commercial silicon solar to become 25% efficient, compared to the 13% efficiency of silicon solar cells employed in PV-RO systems today. Greater improvements will be obtained using more advanced technologies such as multi-junction devices.

## 4. The rankine cycle subsystem

An alternative to PV-RO desalination is the solar-thermal powered RO which typically employs the Rankine cycle. In the Rankine cycle, the working fluid is evaporated in a boiler. Then the generated vapour is adiabatically expanded through a turbine (or other expansion device) to generate mechanical work. The remaining vapour is cooled and condensed to liquid and pumped back to the boiler and the cycle starts again. The working fluid flows in a closed circuit and its volume and pressure change during the Rankine cycle operation as illustrated in Fig. 14 (see reference [64]). The efficiency of a Rankine cycle is less than that of the ideal Carnot cycle.

Since it is a reliable method of power production, the Rankine cycle has been applied for various purposes for decades, such as electricity generation (which is the conventional application of Rankine cycle) and others like vapour compression chillers, water pumping for irrigation or water distribution and so on [82]. Delgado-Torres gave a recent comprehensive review about solar-thermal heat engines for water pumping [83]. Besides solar-thermal energy, the application of Rankine cycle is power generation by biomass combustion and geothermal plants [84]. The emerging applications of the Rankine cycle include waste heat recovery from biogas digestion plants and micro combined heat and power generation and, of course, RO desalination. Nevertheless, except for small water pumping systems, none of these emerging applications has been thoroughly analysed or developed and very few implementations exist [85].

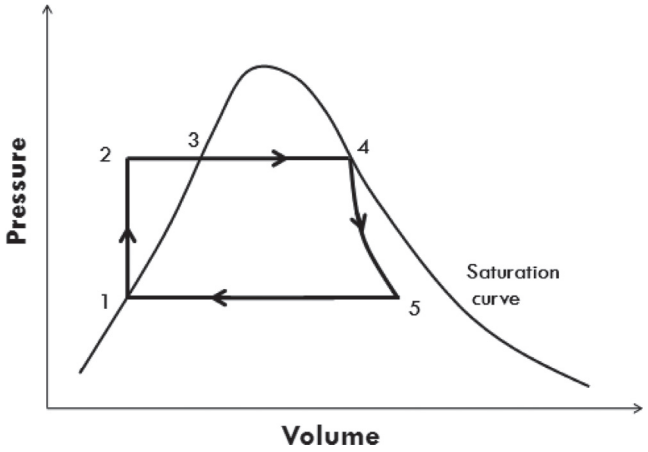


Fig. 14. The volume and pressure changes of working fluid during Rankine cycle operation. Line 1–2 represents the compression of the working fluid by the feed pump to the boiler. Line 2–4 indicates the vaporization of the working fluid at constant pressure. Line 4–5 refers to the steam expansion in the turbine, and then line 5–1 represents the condensation of the vapour-liquid mixture at constant pressure.

### 4.1. Solar desalination with rankine cycle

Fig. 15 illustrates the diagram of a basic solar Rankine cycle-RO system which includes an energy recovery concept in the sense that it preheats the feed water with the heat rejected from the Rankine cycle. The generated mechanical power is used to drive the high pressure pump in the RO sub-system.

There are two main types of solar Rankine cycle configurations: (i) direct vapour generation (DVG) configuration where the working fluid flows directly through the solar collectors and (ii) heat transfer fluid (HTF) configuration where a heating fluid circulates in the solar

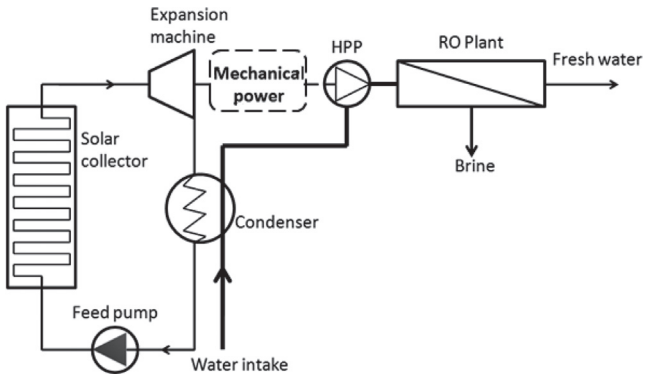


Fig. 15. Schematic of solar-powered Rankine cycle RO system.

collectors, transferring the heat energy to working fluid through a heat exchanger.

Although power generation based on medium temperature solar-thermal collectors combined with the Rankine cycle is well established for power generation around tens of MW, the application of the Rankine cycle to RO desalination is still at an early stage of study and development; consequently the relevant knowledge and experience are very scarce [86]. Among the few published studies on the design and simulation of solar Rankine cycle driven RO desalination shown in Table 4, only three solar heat engine-driven RO systems have been implemented.

The first design study of solar-thermal energy powered RO desalination was that of Bowman et al. and was focussed on Saudi Arabia [95]. Their design was small in size, and intended for producing fresh water from brackish water with a salinity of 5400 ppm. The system consisted of an array of line-focus parabolic trough collectors (PTC), thermal storage backup and reciprocating steam engines which provide mechanical energy to the RO unit high pressure pump and the electrical generator. Simulation results showed that the system could produce a total of 200 l fresh water for unit square meter of collector area (l/m$^2$) for an average March day. The remarkable feature of this system is the thermal storage backup which consists of a steam accumulator feeding the piston engines. This technology balances the thermal energy between the heat source and the heat load, ensuring the system can run continuously under variable operation conditions such as varying solar irradiance during the day.

At the same time, Maurel reported a pilot solar thermal desalination system operated in 1979 at Cadarache in the south of France [96]. It was connected to a 3 kW thermodynamic motor, producing 15 m$^3$ of fresh water from 2000 ppm brackish water a day. Since then, in 1981, Libert and Maurel installed a larger system with a 10 kW solar motor in Egypt which could produce 130 l/m$^2$ per day from 3000 ppm brackish water, and had a 2.2% thermodynamic efficiency [87]. More recently, Manolakos et al. conducted a solar Rankine cycle -RO desalination experiment under real world conditions-at Marathon village, Greece [93]. The system used 88 m$^2$ solar evacuated tube collectors and was capable of producing 80 and 140 l/m$^2$ fresh water on a cloudy and sunny day respectively. The expander efficiencies were 15% and 29% and the Rankine engine efficiencies are 0.73% and 1.17% on a cloudy and sunny day respectively. These values are much lower than the corresponding design study under laboratory conditions, when then expander had 75% efficiency and Rankine engine gave 7% efficiency.

Since the Rankine Cycle requires a working fluid, solar collectors and an expansion system, its efficiency is directly affected by each of its components. Consequently, each component will now be discussed.

### 4.2. Working fluids

One of the most attractive topics as regards improving the Rankine cycle performance is the selection of working fluid. The Rankine cycle's efficiency is strongly affected by the difference between evaporation temperature and condensation temperature, which are highly related to the thermal properties of the fluid. Additionally, environmental issues about various working fluids should be considered carefully. This is why researchers have been searching and selecting the most appropriate working fluids for decades [97–100].

Water is the conventional working fluid for Rankine cycles. Other types of inorganic fluids (e.g., ammonia) have also been used. However water has some weaknesses, such as low molecular weight, and the moisture content of steam may be too high leading to the erosion of the turbine blades. To overcome the shortcomings of the steam-based Rankine cycle, organic working fluids can be utilised such as freons, butane, propane, and other new environmentally friendly refrigerants. Their higher molecular weights lead to slower rotations of the turbines, while lowering the pressure and erosion of the metallic parts and blades. It has been found that for low-temperature levels of heat source, the system will be more efficiently with the use of organic working fluids instead of water [101,102]. Moreover, because of the different critical temperatures and pressures of various organic compounds, the organic Rankine cycle can be utilized for different heat sources of low energy and temperature levels, for instance solar thermal, geothermal, biomass or waste heat from various industries [103,104].

In the last few years, siloxanes have shown themselves to be advantageous as working fluids for low-temperature Rankine cycles. Compared to other organic working fluids, they have higher molecular weight, better stability and lower toxicity [105]. Benzene is also a favourable working fluid regarding its performance, but it exhibits toxicity problems. The conclusions concerning the best working fluids for Rankine cycle-RO systems are controversial. Delgado-Torres and Garcia-Rodriguez presented a working fluid selection study for the low-temperature Rankine cycle coupled with RO desalination [106]. After considering the thermodynamic efficiencies of 12 working fluids with their environmental characterizes and unit aperture area factors, 4 fluids were selected: isopentane, isobutene, R245ca and R245fa. For a heat transfer fluid (HTF) configuration Rankine cycle, isopentane is the best fluid which gave the highest Rankine cycle thermal efficiency of 10–16.6%

Table 4
Overview of solar RC-RO systems

| Authors, date and source | Feed water type | System configuration | Solar collector type | Working fluid | Fresh water production (l/m$^2$ per day) | RC thermal efficiency (%) |
|---|---|---|---|---|---|---|
| Libert et al., 1981 [87] | BW | – | FPC | Freon | 130 | 2.2 |
| Manolakos et al., 2009 [88] | SW | HTF | ETC | HFC-134a | 80–140 | 0.73–1.17 |
| Delgado-Torres et al., 2010[d] [89] | SW | – | CPC | R245fa | 504–744 | 9–12 |
| | | | FPC | | 552–960 | 9–13 |
| | | | ETC | | 984–1224 | 13.5–16 |
| | BW | – | CPC | | 1782–2600 | 9–12 |
| | | | FPC | | 1920–3310 | 9–13 |
| | | | ETC | | 3408–4752 | 13.5–16 |
| Delgado-Torres et al., 2007[d] [90,91] | – | DVG | PTC | Toluene | – | 21 |
| | | | | D4 | – | 19 |
| | | | | MM | – | 18 |
| | | HTF | | Toluene | – | 14–20.6 |
| | | | | D4 | – | 12–18.3 |
| | | | | MM | – | 10–17 |
| Delgado-Torres et al., 2007[d] [92] | SW | DVG | PTC | Toluene | 1800–2640 | 23–32 |
| | | | | D4 | 1200–2160 | 16–27 |
| | | | | MM | 1200–2160 | 15–26 |
| | | HTF | | Toluene | 1540–2400 | 23–30 |
| | | | | D4 | 1080–1848 | 15–27 |
| | | | | MM | 1130–1780 | 15–25 |
| Manolakos et al., 2005[d] [93] | SW | HTF | ETC | HFC-134a | 240 | 7 |
| Nafey and Sharaf, 2010[d] [86] | SW | DVG | FPC | Butane | 166 | 8–8.1 |
| | | | | Water | 188–192 | 9–10 |
| | | | PTC | Toluene | 520 | 25.8–26 |
| | | | | Water | 590–600 | 30–30.5 |
| | | | CPC | Hexane | 200–230 | 14–14.5 |
| | | | | Water | 220–280 | 13–18 |
| Burno et al., 2008[d] [94] | SW | HTF | FPC | Octafluoropropan | 21–30 | 8 |
| | | | ETC | R-245 | 42–53 | 13.3 |
| | | | PTC | Isopentane/ N-prpylbenzene | 75–260 | 28/32 |
| | BW | | FPC | Octafluoropropan | 60–100 | 8 |
| | | | ETC | R-245 | 140–170 | 13.3 |
| | | | PTC | Isopentane/ N-prpylbenzene | 170–830 | 28/32 |

HTF=heat transfer fluid configuration; DVG=direct vapour generation configuration; CPC=compound parabolic collector; FPC=flat plate collector; ETC=evacuated tube collector; PTC=parabolic trough collector; VTC=vacuum tube solar collector; HFC-134a=1,1,1,2-Tetrafluoroethane; R245fa=1,1,1,3,3-Pentafluoropropane;D4=Octamethylcyclotetrasiloxane; MM=Hexamethyldisiloxane; [d]=design study.

and the lowest unit aperture area no matter what type of solar collector was used. Delgado-Torres and Garcia-Rodriguez also pointed out that the size of Rankine cycle-RO compounds, such as the vapour turbine and the condenser, are affected by the choice of working fluid [106]. They found out that for the same power output, the smallest devices were with isobutene as the working fluid whereas isopentane would yield the biggest devices.

Kosmadakis and Manolakos also presented a working fluid selection study for the top cycle of a high temperature two-stage Rankine cycle-RO system [107]. The study considered 33 organic working fluids. After a selection which was not only based on their thermodynamic performances but also various criteria, the most appropriate working fluid found was R245fa.

There is no certain answer as to which working fluid is the most suitable for a Rankine cycle -RO system, since the working fluid cannot be optimised in isolation from the rest of the system. For instance, the solar collector efficiency will be decreased by increasing the evaporation temperature of the working fluid. But if the expansion system is a steam turbine, dry fluids and superheating the fluid are necessary. Besides those mentioned above, the application, size of the system, operation time and conditions should also be considered.

### 4.3. Solar thermal collector

Currently, there are several solar collectors available on the market: the compound parabolic collector (CPC), the flat plate collector (FPC), the parabolic trough collector (PTC) and the evacuated tube collector (ETC). Their efficiency parameters are given in Table 5.

To provide good efficiency in the Rankine cycle, solar collectors must be chosen to suit the operating conditions. As the Rankine cycle can be utilized for different temperatures, all these types of solar collector can be suitable. For electricity generation purpose, high temperature solar collectors are usually preferred such as the parabolic trough collectors (PTC). For solar Rankine cycle-RO systems, research has been carried out to compare the performances of these solar collectors in the Rankine system as shown in Table 4.

In the study of Delgado-Torres and García-Rodriguez, the ETC coupled with R245fa as working fluid showed the best Rankine cycle thermal efficiency of 16%. In another study, Nafey and Sharaf reported that by using the parabolic trough collector with either toluene or water, the system could yield more than 25% efficiency [86]. Based on these limited simulation and design studies, the PTC can be considered as the best choice for the Rankine cycle-RO system due to its high efficiency and high operating temperature.

Table 5
Efficiency parameters for different collector types, from [86]

| Solar collector | Collector optical efficiency ($\eta_{co}$) | Operating temperature (°C) |
|---|---|---|
| FPC | 0.768 | 80–100 |
| CPC | 0.665 | 120–170 |
| PTC | 0.75 | 170–300 |
| ETC | 0.755 | 130–270 |

### 4.4. Expansion device

The most important component of a Rankine cycle is the expansion device since its efficiency affects the system performance directly. Turbines though mostly used in the power range above 50 kW, may not be suitable for smaller systems due to poor efficiency. Other displacement machines such as scroll expanders are also promising [108,109]. The scroll expander is a modification of a compressor commonly used for air conditioning technologies. Other types of expansion device such as rotary Wankel engine and reciprocating steam engine have also been studied [110,111]. The major challenge for the expansion device is the size effect: small devices tend to have large heat losses and thus low conversion efficiencies.

Although the experience with the Rankine cycle coupled to RO desalination is limited, such systems potentially offer numerous advantages like great flexibility, automatic and continuous operation, low maintenance requirements, long lifetime and the ability to recover low to medium grades of input heat. The results presented in Table 4 may not look attractive at first sight, but they are comparable with PV-RO systems which have usually given around 13% efficiency of solar-electricity conversion [105]. From the economic point of view, the specific total cost of a PV-RO system varies between 4.8–7.7 €/m$^3$ depending on battery availabilities, compared to 6.85–12.53 €/m$^3$ for solar Rankine cycle-RO systems [112,113]. However, solar Rankine cycle-RO systems have great potential for cost reduction through further development and commercialisation. In addition, Garcia-Rodriguez and Delgado-Torres pointed out that the SEC of the RO process driven by the Rankine cycle is lower than PV-RO systems and solar distillation as well; thus solar Rankine cycle-RO systems hold promising features for seawater and brackish water desalination for rural communities without access to electricity [105].

## 5. Conclusions

Due to the natural abundance of solar energy, recent advances in solar energy conversion technologies and the low energy consumption of RO desalination, solar-RO (employing either PV or solar thermal conversion) is a reasonable and feasible approach to help tackle the current global water crisis.

With the help of the modern technologies of both RO desalination and solar PVs, many medium and small scale solar PV-RO desalination systems have been implemented in arid or semi-arid areas. They exhibit good performance in terms of their specific electrical energy consumption

which can be as low as 5 kWh/m$^3$. However, this is much higher than the ideal values of 0.15 kWh/m$^3$ for brackish water and 0.94 kWh/m$^3$ for seawater; in this sense their performances are still wanting. For large SWRO systems using high-efficiency ERDs, the energy losses are mainly dependant on membrane resistances which are heavily related to membrane types and conditions. And another aspect is system configuration. By dividing the whole RO module channel into two or more stages in series, the efficiency of the system can be improved up to 20%. This improvement can be much larger for BWRO systems. Due to their low operating pressures and high recovery, these systems rarely employ ERDs. Additionally, the smaller inverters and pumps which are typically adopted in the small or medium brackish water system often have poor efficiencies.

When the PV subsystem is taken into account, the overall efficiencies of PV-RO systems are quite low. The crystalline Si solar cells which are utilized in most PV-RO systems only have around 13% efficiency, which is much lower than the theoretical solar energy conversion limit of 86.8%. In other words, there is still huge room for improvement. Based on the ideal limiting efficiency of solar energy conversion, overall efficiency could theoretically be improved 40 times for PV-SWRO and 200 times for PV-BWRO systems. Of course, some losses are unavoidable in practice, because zero membrane resistance, infinite numbers of RO stages and infinitely stacked solar cells, etc., cannot be achieved. However, with emerging solar cell technologies and R&D into RO membranes, the authors anticipate that PV-SWRO and PV-BWRO systems can be improved by at least 5 and 10 times respectively.

An alternative to the PV-RO system is the solar Rankine cycle-RO system. This is still at the early stage of development, with very few plants having been built. Nevertheless, a few modelling and design studies have been carried out based on different solar collector types and working fluids. In principle, the parabolic trough collector behaves better than other collectors. The choice of working fluid remains controversial. Further analyses regarding the choice of cost effective solar collectors, suitable working fluids and a practical high efficiency expansion device are required. Owing to the promising features of Rankine cycle-RO systems, such as the comparable efficiency and lower cost than PV, more R&D should be conducted to realise their potential.

**Acknowledgements**

The authors would like to acknowledge financial support from the School of Engineering and Applied Science, and the contributions of the colleagues at the Sustainable Environment Research group at Aston University.

**Symbols**

| Symbol | Units | Description |
|---|---|---|
| $C$ | ppm | concentration |
| $D$ | m$^2$/s | diffusion coefficient of salt |
| $J$ | m/s | flux of water permeating the membrane |
| $k$ | m/s | mass transfer coefficient |
| $K$ | — | mixing efficiency of the net |
| $M$ | — | characteristic length of the net |
| $n$ | — | number of RO module stages |
| $P$ | Pa | pressure |
| $Pe$ | — | Peclet number |
| $r$ | — | recovery ratio for each stage |
| $R$ | — | overall recovery ratio |
| $R_0$ | — | salt rejection |
| $Sc$ | — | Schmidt number |
| η | — | efficiency |

*Subscripts*

| | | |
|---|---|---|
| b | — | of bulk solution |
| co | — | of solar collector |
| ideal | — | of ideal case |
| m | — | of membrane |
| osm | — | osmotic |
| p | — | of permeate |
| r | — | ratio |
| solar | — | of solar energy conversion |

*Abbreviations*

| | | |
|---|---|---|
| BW | — | brackish water |
| CP | — | concentration polarization |
| ERD | — | energy recovery device |
| PV | — | photovoltaic |
| RC | — | rankine cycle |
| RES | — | renewable energy source |
| RO | — | reverse osmosis |
| SEC | — | specific energy consumption |
| SW | — | seawater |

**References**

[1] G. Fiorenza, V. Sharma and G. Braccio, Techno-economic evaluation of a solar powered water desalination plant, Energy Convers. Manage., 44(14) (2003) 2217–2240.
[2] E. Mathioulakis, V. Belessiotis and E. Delyannis, Desalination by using alternative energy: Review and state-of-the-art, Desalination, 203(1–3) (2007) 346–365.
[3] C. Fritzmann, J. Löwenberg, T. Wintgens and T. Melin, State-of-the-art of reverse osmosis desalination, Desalination, 216(1–3) (2007) 1–76.
[4] K. Wangnick, IDA Worldwide Desalination Plants Inventory, Report No. 17, Wangnick Consulting GmbH, 2002.
[5] A.M. Delgado-Torres and L. García-Rodríguez, Status of solar thermal-driven reverse osmosis desalination, Desalination, 216(1–3) (2007) 242–251.
[6] B.G. Keeper, R.D. Hembree and F.C. Schrack, Optimized matching of solar photovoltaic power with reverse osmosis desalination, Desalination, 54 (1985) 89–103.

[7] W.T. Andrews, W.F. Pergande and G.S. McTaggart, Energy performance enhancements of a 950 $m^3$/d seawater reverse osmosis unit in Grand Cayman, Desalination, 135(1–3) (2001) 195–204.
[8] A.D. Vos, Detailed balance limit of the efficiency of tandem solar cells, J. Phys. D: Appl. Phys., 13(5) (1980) 839.
[9] http://iom.edu/Reports/2004/Dietary-Reference-Intakes-Water-Potassium-Sodium-Chloride-and-Sulfate.aspx.
[10] A. Al-Karaghouli, D. Renne and L.L. Kazmerski, Technical and economic assessment of photovoltaic-driven desalination systems, Renewable Energy, 35(2) (2010) 323–328.
[11] H.M. Laborde, K.B. Franca, H. Neff and A.M.N. Lima, Optimization strategy for a small-scale reverse osmosis water desalination system based on solar energy, Desalination, 133(1) (2001) 1–12.
[12] E. Mohamed, G. Papadakis, E. Mathioulakis and V. Belessiotis, A direct coupled photovoltaic seawater reverse osmosis desalination system toward battery based systems–a technical and economical experimental comparative study, Desalination, 221(1–3) (2008) 17–22.
[13] E.S. Mohamed, G. Papadakis, E. Mathioulakis and V. Belessiotis, The effect of hydraulic energy recovery in a small sea water reverse osmosis desalination system; experimental and economical evaluation, Desalination, 184(1–3) (2005) 241–246.
[14] D. Herold and A. Neskakis, A small PV-driven reverse osmosis desalination plant on the island of Gran Canaria, Desalination, 137(1–3) (2001) 285–292.
[15] D. Herold, V. Horstmann, A. Neskakis, J. Plettner-Marliani, G. Piernavieja and R. Calero, Small scale photovoltaic desalination for rural water supply-demonstration plant in Gran Canaria, Renewable Energy, 14(1–4) (1998) 293–298.
[16] E. Mohamed and G. Papadakis, Design, simulation and economic analysis of a stand-alone reverse osmosis desalination unit powered by wind turbines and photovoltaics, Desalination, 164(1) (2004) 87–97.
[17] M. Thomson and D. Infield, A photovoltaic-powered seawater reverse-osmosis system without batteries, Desalination, 153(1–3) (2003) 1–8.
[18] E. Tzen, K. Perrakis and P. Baltas, Design of a stand alone PV-desalination system for rural areas, Desalination, 119(1–3) (1998) 327–333.
[19] A. Joyce, D. Loureiro, C. Rodrigues and S. Castro, Small reverse osmosis units using PV systems for water purification in rural places, Desalination, 137(1–3) (2001) 39–44.
[20] G.E. Ahmad and J. Schmid, Feasibility study of brackish water desalination in the Egyptian deserts and rural regions using PV systems, Energy Convers. Manage., 43(18) (2002) 2641–2649.
[21] P.C.M. de Carvalho, D.B. Riffel, C. Freire and F.F.D. Montenegro, The Brazilian experience with a photovoltaic powered reverse osmosis plant, Prog. Photovoltaics, 12(5) (2004) 373–385.
[22] A. De Munari, D.P.S. Capao, B.S. Richards and A.I. Schafer, Application of solar-powered desalination in a remote town in South Australia, Desalination, 248(1–3) (2009) 72–82.
[23] B.S. Richards and A.I. Schafer, Photovoltaic-powered desalination system for remote Australian communities, Renewable Energy, 28(13) (2003) 2013–2022.
[24] D.B. Riffel and P.C.M. Carvalho, Small-scale photovoltaic-powered reverse osmosis plant without batteries: Design and simulation, Desalination, 247(1–3) (2009) 378–389.
[25] K.B. Franca, H.M. Laborde and H. Neff, Design and Performance of Small Scale Solar Powered Water Desalination Systems, Utilizing Reverse Osmosis, J. Sol. Energy Eng., 122(4) (2000) 170–175.
[26] I. Karassik, J. Messina, P. Cooper, C. Heald, W. Krutzsch, A. Hosangadi, C. Kittredge, W. Fraser, W. Marscher and P. Boyadjis, Pump handbook, McGraw-Hill, New York, (2001).
[27] M.W.L.A.C.B.M.M.G.P.N. Voutchkov, The Guidebook to Membrane Desalination Technology : Reverse Osmosis, Nanofiltration and Hybrid Systems Process, Design, Applications and Economics 2007.
[28] D.J. Woodcock and I. Morgan White, The application of pelton type impulse turbines for energy recovery on sea water reverse osmosis systems, Desalination, 39 (1981) 447–458.
[29] Y. Mimura, S. Taniguchi and E. Tatsumura Mashima, How to obtain highest plan efficiency for RO desalination plant, Desalination, 54 (1985) 219–225.
[30] P. Goubeau and P. Leroy, A specific energy recovery pumping system for reverse osmosis desalination, Desalination, 44(1–3) (1983) 199–206.
[31] J. Lozier, E. Oklejas and M. Silbernagel, The hydraulic turbocharger(TM): a new type of device for the reduction of feed pump energy consumption in reverse osmosis systems, Desalination, 75 (1989) 71–83.
[32] M. Silbernagel, T. Kuepper and E. Oklejas, Evaluation of a pressure boosting pump/turbine device for reverse osmosis energy recovery: Extended testing on a seawater desalination system, Desalination, 88(1–3) (1992) 311–319.
[33] P. Geisler, F.U. Hahnenstein, W. Krumm and T. Peters, Pressure exchange system for energy recovery in reverse osmosis plants, Desalination, 118(1–3) (1998) 91–91.
[34] B. Peñate, J.A. de la Fuente and M. Barreto, Operation of the RO Kinetic® energy recovery system: Description and real experiences, Desalination, 252(1–3) (2010) 179–185.
[35] R. Stover and I. Cameron, Energy Recovery in Caribbean Seawater Reverse Osmosis, 2007.
[36] R. Stover, Seawater reverse osmosis with isobaric energy recovery devices, Desalination, 203(1–3) (2007) 168–175.
[37] J. MacHarg, Retro-fitting existing SWRO systems with a new energy recovery device, Desalination, 153(1–3) (2003) 253–264.
[38] http://www.energyrecovery.com/.
[39] R.L. Stover, A. Ameglio and P.A.K. Khan, The Ghalilah SWRO plant: an overview of the solutions adopted to minimize energy consumption, Desalination, 184(1–3) (2005) 217–221.
[40] U. Merten, Flow Relationships in Reverse Osmosis, Ind. Eng. Chem. Fundam., 2(3) (1963) 229–232.
[41] P.L.T. Brian, Concentration Polar zation in Reverse Osmosis Desalination with Variable Flux and Incomplete Salt Rejection, Ind. Eng. Chem. Fundam., 4(4) (1965) 439–445.
[42] J.E. Flinn, ed., Membrane Science and Technology, ed., A.D.W. Blatt, A.S. Michaels and L. Nelsen, 1970, Plenum, 47–91.
[43] M.C. Porter, Concentration Polarization with Membrane Ultrafiltration, Product R&D, 11(3) (1972) 234–248.
[44] G.A. Denisov, Theory of concentration polarization in crossflow ultrafiltration: gel-layer model and osmotic-pressure model, J. Membr. Sci., 91(1–2) (1994) 173–187.
[45] L. Song and M. Elimelech, Theory of concentration polarization in crossflow filtration, J. Chem. Soc., Faraday Trans., 91 (1995).
[46] I. Sutzkover, D. Hasson and R. Semiat, Simple technique for measuring the concentration polarization level in a reverse osmosis system, Desalination, 131(1–3) (2000) 117–127.
[47] S. Sourirajan, Reverse Osmosis, (1970) 180-189, UK, Logos Press Ltd.
[48] E. Matthiasson and B. Sivik, Concentration polarization and fouling, Desalination, 35 (1980) 59–103.
[49] V. Gekas and B. Hallström, Mass transfer in the membrane concentration polarization layer under turbulent cross flow : I. Critical literature review and adaptation of existing sherwood correlations to membrane operations, J. Membr. Sci., 30(2) (1987) 153–170.
[50] A. Chiolle, G. Gianotti, M. Gramondo and G. Parrini, Mathematical model of reverse osmosis in parallel-wall channels with turbulence promoting nets, Desalination, 26(1) (1978) 3–16.
[51] M.B. Boudinar, W.T. Hanbury and S. Avlonitis, Numerical simulation and optimisation of spiral-wound modules, Desalination, 86(3) (1992) 273–290.
[52] M.F.A. Goosen, S.S. Sablani, S.S. Al-Maskari, R.H. Al-Belushi and M. Wilf, Effect of feed temperature on permeate flux and mass transfer coefficient in spiral-wound reverse osmosis systems, Desalination, 144(1–3) (2002) 367–372.
[53] A. Luque and S. Hegedus, Handbook of photovoltaic science and engineering, John Wiley & Sons Inc. (2003).
[54] M. Green, Third generation photovoltaics: advanced solar energy conversion, Springer Verlag (2003).
[55] D. Trivich and P. Flinn, Maximum Efficiency of Solar Energy Conversion by Quantum Process, Solar Energy Research, University of Wisconsin Press, Madison, Wis., sec. VI, 1953: p. 143–147.

[56] W. Shockley and H. Queisser, Detailed Balance Limit of Efficiency of p n Junction Solar Cells, J. Appl. Phys., 32 (1961) 510.
[57] C. Mathers, Upper limit of efficiency for photovoltaic solar cells, J. Appl. Phys., 48 (1977) 3181.
[58] W. Ruppel and P. Wurfel, Upper limit for the conversion of solar energy, Electron Devices, IEEE Transactions on, 27(4) (1980) 877–882.
[59] N.A. Gokcen and J.J. Loferski, Efficiency of tandem solar cell systems as a function of temperature and solar energy concentration ratio, Sol. Energy Mater., 1(3–4) (1979) 271–286.
[60] R. Brendel, J.H. Werner and H.J. Queisser, Thermodynamic efficiency limits for semiconductor solar cells with carrier multiplication, Sol. Energy Mater. Sol. Cells, 41–42 (1996) 419–425.
[61] A. De Vos and J. Bekaert, Endoreversible thermodynamics of solar energy conversion, Oxford University Press, Oxford (1992).
[62] G.L. Araújo and A. Martí, Absolute limiting efficiencies for photovoltaic energy conversion, Sol. Energy Mater. Sol. Cells, 33(2) (1994) 213–240.
[63] R. Wengenmayr and T. Bührke, Renewable energy: sustainable energy concepts for the future, Vch Verlagsgesellschaft Mbh (2008).
[64] M. Kettani, Direct energy conversion, Addison-Wesley Publ. Co., Menlo Park, CA (1970).
[65] J. Zhao, A. Wang, M. Green and F. Ferrazza, 19.8% efficient ``honeycomb'' textured multicrystalline and 24.4% monocrystalline silicon solar cells, Appl. Phys. Lett., 73(14) (1998) 1991–1993.
[66] M.A. Green, K. Emery, Y. Hishikawa and W. Warta, Solar cell efficiency tables (version 35), Prog. Photovoltaics Res. Appl., 18(2) (2010) 144–150.
[67] P. Lynn, Electricity from Sunlight, 2010.
[68] C. Algora, E. Ortiz, I. Rey-Stolle, V. Diaz, R. Pena, V.M. Andreev, V.P. Khvostikov and V.D. Rumyantsev, A GaAs solar cell with an efficiency of 26.2% at 1000 suns and 25.0% at 2000 suns, Electron Devices, IEEE Transactions on, 48(5) (2001) 840–844.
[69] A.W. Bett, F. Dimroth, G. Lange, M. Meusel, R. Beckert, M. Hein, S.V. Riesen, and U. Schubert, 30% monolithic tandem concentrator solar cells for concentrations exceeding 1000 suns, In Photovoltaic Specialists Conference, 2000, Conference Record of the Twenty-Eighth IEEE, 2000.
[70] J. Nelson, The physics of solar cells, World Scientific Pub Co Inc. (2003).
[71] M.A. Green, Limits on the open-circuit voltage and efficiency of silicon solar cells imposed by intrinsic Auger processes, Electron Devices, IEEE Transactions on, 31(5) (1984) 671–678.
[72] M. Saad and A. Kassis, Effect of interface recombination on solar cell parameters, Sol. Energy Mater. Sol. Cells, 79(4) (2003) 507–517.
[73] L.A. Kosyachenko, E.V. Grushko and V.V. Motushchuk, Recombination losses in thin-film CdS/CdTe photovoltaic devices, Sol. Energy Mater. Sol. Cells, 90(15) (2006) 2201–2212.
[74] T. Markvart, Solar electricity, John Wiley & Sons Inc. (2000).
[75] T. Lauinger, J. Schmidt, A. Aberle and R. Hezel, Record low surface recombination velocities on 1 cm p silicon using remote plasma silicon nitride passivation, Appl. Phys. Lett., 68 (1996) 1232.
[76] P.E. Gruenbaum, J.Y. Gan, R.R. King and R.M. Swanson, Stable passivations for high-efficiency silicon solar cells, In Photovoltaic Specialists Conference, 1990, Conference Record of the Twenty First IEEE, 1990.
[77] M. Cid, N. Stem, C. Brunetti, A. Beloto and C. Ramos, Improvements in anti-reflection coatings for high-efficiency silicon solar cells, Surf. Coat. Technol., 106(2–3) (1998) 117–120.
[78] J. Zhao, A. Wang, M. Green and F. Ferrazza, 19.8% efficient "honeycomb" textured multicrystalline and 24.4% monocrystalline silicon solar cells, Appl. Phys. Lett., 73 (1998) 1991.
[79] R. Hezel, A new high efficiency solar cell concept based on truncated pyramids, In Photovoltaic Energy Conversion, 1994, Conference Record of the Twenty Fourth IEEE Photovoltaic Specialists Conference - 1994, 1994 IEEE First World Conference on, 1994.
[80] T. Juvonen and et al., High Efficiency Single Crystalline Silicon Solar Cells, Phys. Scr., 2002(T101) 96.
[81] A. Yoshikawa and H. Kasai, Optimum design for window layer thickness of GaAlAs‐GaAs heteroface solar cell regarding the effect of reflection loss, J. Appl. Phys., 52(6) (1981) 4345–4347.
[82] M. Aghamohammadi, J. Zarinchang and M. Yaghoubi, Performance of a Solar Water Pump In Southern Part of Iran, 2001.
[83] A. Delgado-Torres, Solar thermal heat engines for water pumping: an update, Renewable Sustainable Energy Rev., 13(2) (2009) 462–472.
[84] A. Schuster, S. Karellas, E. Kakaras and H. Spliethoff, Energetic and economic investigation of Organic Rankine Cycle applications, Appl. Therm. Eng., 29(8–9) (2009) 1809–1817.
[85] L. García-Rodríguez and J. Blanco-Gálvez, Solar-heated Rankine cycles for water and electricity production: POWERSOL project, Desalination, 212(1–3) (2007) 311–318.
[86] A.S. Nafey and M.A. Sharaf, Combined solar organic Rankine cycle with reverse osmosis desalination process: Energy, exergy, and cost evaluations, Renewable Energy, 35(11) (2010) 2571–2580.
[87] J.J. Libert and A. Maurel, Desalination and renewable energies-a few recent developments, Desalination, 39 (1981) 363–372.
[88] D. Manolakos, G. Kosmadakis, S. Kyritsis and G. Papadakis, On site experimental evaluation of a low-temperature solar organic Rankine cycle system for RO desalination, Sol. Energy, 83(5) (2009) 646–656.
[89] A.M. Delgado-Torres and L. García-Rodríguez, Preliminary design of seawater and brackish water reverse osmosis desalination systems driven by low-temperature solar organic Rankine cycles (ORC), Energy Convers. Manage., 51(12) (2010) 2913–2920.
[90] A. Delgado-Torres and L. García-Rodríguez, Preliminary assessment of solar organic Rankine cycles for driving a desalination system, Desalination, 216(1–3) (2007) 252–275.
[91] A.M. Delgado-Torres and L. García-Rodríguez, Comparison of solar technologies for driving a desalination system by means of an organic Rankine cycle, Desalination, 216(1–3) (2007) 276–291.
[92] A. Delgado-Torres, L. García-Rodríguez and V. Romero-Ternero, Preliminary design of a solar thermal-powered seawater reverse osmosis system, Desalination, 216(1–3) (2007) 292–305.
[93] D. Manolakos, , G. Papadakis, E.S. Mohamed, S. Kyritsis and K. Bouzianas, Design of an autonomous low-temperature solar Rankine cycle system for reverse osmosis desalination, Desalination, 183(1–3) (2005) 73–80.
[94] J. Bruno, J. López-Villada, E. Letelier, S. Romera and A. Coronas, Modelling and optimisation of solar organic Rankine cycle engines for reverse osmosis desalination, Appl. Therm. Eng., 28(17–18) (2008) 2212–2226.
[95] T. Bowman, A. El-Nashar, B. Thrasher, A. Husseiny and A. Unione, Design of a small solar-powered desalination system, Desalination, 39 (1981) 71–81.
[96] A. Maurel, Dessalement et energies nouvelles, Desalination, 31(1–3) (1979) 489–499.
[97] B. Saleh, G. Koglbauer, M. Wendland and J. Fischer, Working fluids for low-temperature organic Rankine cycles, Energy, 32(7) (2007) 1210–1221.
[98] B.F. Tchanche, G. Papadakis, G. Lambrinos and A. Frangoudakis, Fluid selection for a low-temperature solar organic Rankine cycle, Appl. Therm. Eng., 29(11–12) (2009) 2468–2476.
[99] O. Badr, S.D. Probert and P.W. O'Callaghan, Selecting a working fluid for a Rankine-cycle engine, Appl. Energy, 21(1) (1985) 1–42.
[100] G. Angelino and P. Colonna di Paliano, Multicomponent Working Fluids For Organic Rankine Cycles (ORCs), Energy, 23(6) (1998) 449–463.
[101] B. Liu, K. Chien and C. Wang, Effect of working fluids on organic Rankine cycle for waste heat recovery, Energy, 29(8) (2004) 1207–1217.
[102] T. Yamamoto, T. Furuhata, N. Arai and K. Mori, Design and testing of the organic Rankine cycle Energy, 26(3) (2001) 239–251.

[103] H. Madhawa Hettiarachchi, M. Golubovic, W. Worek and Y. Ikegami, Optimum design criteria for an organic Rankine cycle using low-temperature geothermal heat sources, Energy, 32(9) (2007) 1698–1706.
[104] V. Maizza and A. Maizza, Unconventional working fluids in organic Rankine-cycles for waste energy recovery systems, Appl. Therm. Eng., 21(3) (2001) 381–390.
[105] L. García-Rodríguez and A. Delgado-Torres, Solar-powered Rankine cycles for fresh water production, Desalination, 212(1–3) (2007) 319–327.
[106] A.M. Delgado-Torres and L. García-Rodríguez, Analysis and optimization of the low-temperature solar organic Rankine cycle (ORC), Energy Convers. Manage., 51(12) (2010) 2846–2856.
[107] G. Kosmadakis, D. Manolakos, S. Kyritsis and G. Papadakis, Comparative thermodynamic study of refrigerants to select the best for use in the high-temperature stage of a two-stage organic Rankine cycle for RO desalination, Desalination, 243(1–3) (2009) 74–94.
[108] V. Lemort, S. Quoilin, C. Cuevas and J. Lebrun, Testing and modeling a scroll expander integrated into an Organic Rankine Cycle, Appl. Therm. Eng., 29(14–15) (2009) 3094–3102.
[109] S. Quoilin, V. Lemort and J. Lebrun, Experimental study and modeling of an Organic Rankine Cycle using scroll expander, Appl. Energy, 87(4) (2010) 1260–1268.
[110] O. Badr, S. Naik, P.W. O'Callaghan and S.D. Probert, Rotary Wankel engines as expansion devices in steam Rankine-cycle engines, Appl. Energy, 39(1) (1991) 59–76.
[111] M. Badami and M. Mura, Preliminary design and controlling strategies of a small-scale wood waste Rankine Cycle (RC) with a reciprocating steam engine (SE), Energy, 34(9) (2009) 1315–1324.
[112] D. Manolakos, E.S. Mohamed, I. Karagiannis and G. Papadakis, Technical and economic comparison between PV-RO system and RO-Solar Rankine system. Case study: Thirasia island, Desalination, 221(1–3) (2008) 37–46.
[113] G. Kosmadakis, D. Manolakos, S. Kyritsis and G. Papadakis, Economic assessment of a two-stage solar organic Rankine cycle for reverse osmosis desalination, Renewable Energy, 34(6) (2009) 1579–1586.